JOURNAL OF COMPUTATIONAL PHYSICS **125,** 26–41 (1996)
ARTICLE NO. 0077

A Numerical Model for the Simulation of Quench in the ITER Magnets

L. BOTTURA*

CERN, Division LHC, CH-1211 Geneva 23, Switzerland

Received December 15, 1994; revised June 26, 1995

A computational model describing the initiation and evolution of normal zones in the cable-in-conduit superconductors designed for the international thermonuclear experimental reactor (ITER) is presented. Because of the particular geometry of the ITER cables, the model treats separately the helium momenta in the two cooling channels and the temperatures of the cable constituents. The numerical implementation of the model is discussed in conjunction with the selection of a well-suited solution algorithm. In particular, the solution procedure chosen is based on an implicit upwind finite element technique with adaptive time step and mesh size adjustment possibilities. The time step and mesh adaption procedures are described. Examples of application of the model are also reported.

1. INTRODUCTION

The international thermonuclear experimental reactor (ITER [1]), the most probable next step large scale experiment for magnetically confined fusion, will have supercritical-helium, force-flow cooled superconducting magnets forming a considerable part of the basic tokamak structure. The magnets will be wound using so-called *cable-in-conduit conductors* (CICCs) in unit lengths ranging between 750 and 1500 m. A CICC consists of a bundle of cabled superconducting and copper strands jacketed in a helium tight conduit with primary structural function (i.e., support for the Lorentz force). Helium, at about 4.5 K inlet temperature, flows in the spaces within the strands and maintains the cable temperature sufficiently below the maximum allowed by the superconducting material (called the *critical* temperature T_c of the superconductor at the working conditions of transport current and background magnetic field). A typical CICC's prototype built in the frame of the ITER R & D programme is shown in Fig. 1.

In DC conditions the magnet is superconducting and thus operates with zero resistance, i.e., no Joule dissipation. However, due to local (and not foreseen) heat inputs, a section of the cable could increase its temperature above T_c, where the superconductor develops a resistance. In this so-called *normal* zone the current is shared between the superconductor and the copper, functioning as a shunt. In this case Joule heating takes place in the normal zone and the compressible, heated helium is expelled. Because of conduction at the ends of the normal zone and heat convection through the helium expulsion, the normal zone propagates in the magnet. The detection of a resistance in the magnet usually triggers protection systems which disconnect the power supply and discharge the magnetic energy (of the order of 100 GJ in the ITER toroidal field system [1]) onto external resistors. This process is usually called a *quench* of the magnet.

From the point of view of the design and analysis of a superconducting magnet [2] it is interesting to predict the evolution of the quench. In particular, the main issues are the maximum temperature and pressure in the cable (used to verify mechanical stresses due to differential thermal expansion and pressure load), the helium expulsion (to size the venting lines), and the normal zone propagation velocity and voltage (in order to set a threshold and requirements on the sensitivity for the detection of a normal region). Mainly for analysis purposes, several models were developed in the past years [3–7]. The numerical solutions were based on a variety of methods, ranging from collocation packages [3, 7], to time-explicit finite elements (Taylor–Galerkin) procedure [4], method of lines [5], and finite differences in conjunction with an ODE integrator in time [6]. This variety of methods witnesses the difficulties in the establishment of a well-optimised procedure. In fact, for none of them a coherent rationale was given for the selection of the solution procedure.

In particular, the analytical and numerical approach of Ref. [7] has shown that the physical characteristics of the moving normal front in the superconducting cable can lead to significant difficulties in obtaining accurate simulations. The use of a mesh adaption technique was proposed there in order to improve the accuracy of the results at acceptable memory/CPU requirements. In Ref. [8] it has been shown that the presence of sharp boundary layers in the solution

* E-mail: botturl@mt.msm.cern.ch.

0021-9991/96 $18.00

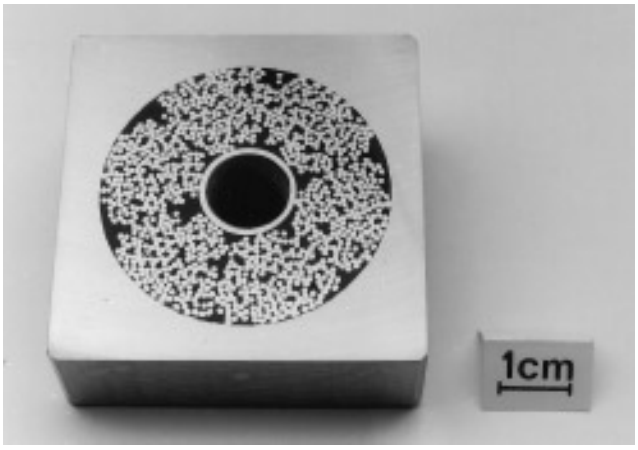

FIG. 1. Prototype of a 40 kA CICC developed for fusion application in the Central Solenoid coil of the ITER experiment.

at the normal front imposes requirements to the mesh size and time step to be used in the analysis, in addition to those arising naturally from the numerical method chosen.

The purpose of this work is to discuss the features of the implementation of a model proposed for the quench propagation in the ITER CICCs. In Section 2 the equations forming the model are presented, Section 3 deals with the selection of the method and the numerical implementation, and, finally, in Section 4 experimental data are compared to the results of numerical simulations.

As is shown in Fig. 1, the ITER CICC design has the peculiarity of a central cooling hole, separated from the cable bundle by a spiral or a perforated pipe, to allow large massflows under reduced friction compared to simpler CICCs without a hole. Because of the lower hydraulic resistance of the cooling hole, the helium flow is expected to have a higher velocity in the hole compared to the cable bundle. This difference changes the dynamics of the flow and of the heat transfer between the cable and the cooling helium. Therefore some effort is spent initially in the presentation of a model for a CICC with a dual cooling channel.

2. MODEL FOR THE QUENCHING CICC

The quench initiation and propagation in a CICC can be described in a first approximation using a 1D schematization of the cable which ignores the size of the cable cross section compared to the longitudinal cable length (see Ref. [4] and the references quoted there). This is a good approximation for existing magnets, as the cable lengths are of the order of several hundreds of meters to be compared to transverse dimensions of the order of some centimeters. Temperature gradients in the cable cross section cannot be fully ignored, as a full homogenization of the thermal properties would lead to an overestimate of the thermal capacity of the cable ignoring the time lag in the temperature history. A compromise solution, as chosen in [4], is to treat separately the strands in the cable, the helium, and the outer conduit. The evolution of the system in time (t) is then described by the mass, momentum, and energy balances in the helium and the heat diffusion in the strands and conduit in the direction of the flow path (x). Coupling the equations is obtained through convective heat fluxes at the wetted or contact surfaces. Particular attention is to be devoted to the non-linearities of the problem, i.e., strong variations of the thermal properties, heat transfer coefficient, or the onset of the Joule heat generation term. In the next sections the equations describing the system are presented.

2.1. *Two Channels Helium Flow*

According to the results of Ref. [9], summarised in Appendix A, it is possible to assume that in the time scale of interest for the quench propagation the helium thermodynamic state is the same in the cable bundle and in the cooling hole (*perfect mixing* hypothesis); i.e., in particular the helium pressure and temperature is uniform in the cross section of the cable. This allows a significant simplification in the conservation balances. Assuming in addition that no momentum is transferred among the two flows, the helium state and motion is described by the following set of equations (see Appendix A for details) for the pressure p, the temperature T_{He} and the flow velocities in the cable bundle (v_{B}) and in the cooling hole (v_{H}):

$$\frac{\partial v_{\mathrm{B}}}{\partial t} + v_{\mathrm{B}}\frac{\partial v_{\mathrm{B}}}{\partial x} + \frac{1}{\rho}\frac{\partial p}{\partial x} = -F_{\mathrm{B}} \tag{1}$$

$$\frac{\partial v_{\mathrm{H}}}{\partial t} + v_{\mathrm{H}}\frac{\partial v_{\mathrm{H}}}{\partial x} + \frac{1}{\rho}\frac{\partial p}{\partial x} = -F_{\mathrm{H}} \tag{2}$$

$$\frac{\partial p}{\partial t} + a_{\mathrm{B}}\rho c^2\frac{\partial v_{\mathrm{B}}}{\partial x} + a_{\mathrm{H}}\rho c^2\frac{\partial v_{\mathrm{H}}}{\partial x} + v\frac{\partial p}{\partial x} = \phi(a_{\mathrm{B}}v_{\mathrm{B}}F_{\mathrm{B}} + a_{\mathrm{H}}v_{\mathrm{H}}F_{\mathrm{H}}) + \frac{\phi Q_{\mathrm{He}}}{A_{\mathrm{He}}} \tag{3}$$

$$\frac{\partial T_{\mathrm{He}}}{\partial t} + a_{\mathrm{B}}\phi T_{\mathrm{He}}\frac{\partial v_{\mathrm{B}}}{\partial x} + a_{\mathrm{H}}\phi T_{\mathrm{He}}\frac{\partial v_{\mathrm{H}}}{\partial x} + v\frac{\partial T_{\mathrm{He}}}{\partial x} = \frac{(a_{\mathrm{B}}v_{\mathrm{B}}F_{\mathrm{B}} + a_{\mathrm{H}}v_{\mathrm{H}}F_{\mathrm{H}})}{\rho C_{\mathrm{v}}} + \frac{Q_{\mathrm{He}}}{A_{\mathrm{He}}\rho C_{\mathrm{v}}}, \tag{4}$$

where ρ is the helium density, C_{V} the specific heat at constant volume, c is the isentropic sound speed, and ϕ is the Gruneisen parameter (see Appendix A). Note that the equations obtained above do not introduce any simplification on the helium state, which is treated consistently as a non-perfect, single-phase fluid. The main advantage of

the use of the above non-conservative form is that pressure and temperature appear explicitly as variables. This, as it will be shown in the examples later on, can be used to increase dramatically the stability of the solution algorithm.

Pressure and temperature in the flow are convected at the average velocity v, obtained as the ratio of the total helium flux to the total helium area [9], i.e.,

$$v = a_B v_B + a_H v_H, \tag{5}$$

where a_B and a_H are the fraction of the total heilum area A_{He} in the bundle and hole, respectively,

$$a_B = \frac{A_{HeB}}{A_{He}}; \quad a_H = \frac{A_{HeH}}{A_{He}}.$$

The friction force at the wetted surface is indicated by the terms F_B and F_H, given by

$$F_B = 2 f_B \frac{v_B |v_B|}{D_{hB}} \tag{6}$$

$$F_H = 2 f_H \frac{v_H |v_H|}{D_{hH}}. \tag{7}$$

Different friction factors f_B and f_H and hydraulic diameters D_{hH}, D_{hB} can be assigned to the two flows to better match the hydraulic characteristics of the conductor. Finally, the linear heat source density term Q_{He} is represented by the convective heat flux (in W/m) at the wetted surface of the strands and of the conduit,

$$\begin{aligned} Q_{He} = Q_{He,St} + Q_{He,Jk} = p_{St} h_{St} (T_{St} - T_{He}) \\ + p_{Jk} h_{Jk} (T_{Jk} - T_{He}), \end{aligned} \tag{8}$$

showing the splitting in the contribution of the strands and of the conduit at temperatures T_{St} and T_{Jk} respectively, where p_{St} and p_{Jk} are the wetted perimeters of strand and conduit jacket and h_{St}, h_{Jk} are the corresponding heat transfer coefficients. As a final remark, note that the system of Eqs. (1)–(4) reduces to the common description of CICC's flow without a cooling channel [3–7] when $A_{HeH} = 0$ and $A_{HeB} = A_{He}$ (and eliminating the hole momentum balance, Eq. (2), from the system). This particular case is therefore retained in the present model and will be indeed used for the validation runs presented later on.

2.2. *Strand and Conduit* (*Jacket*)

Heat diffuses in the strands and in the conduit. In addition heat generation can take place either because of external sources or Joule heating. The temperatures of the strands and of the conduit are assumed to be uniform in the cross section but are kept distinct. This assumption is based on the good thermal contact of the strands and of the conduit with the flowing helium and the uniformity of the volumetric heat source. Temperature differences within the cross section of the CICC can be significant only for times comparable with the current redistribution time in the cable, i.e., at most for transients in the time scale of stability and recovery. The helium turbulence tends to decrease these gradients, so that they should become negligible in the time scale of the quench evolution. The equations describing the evolution of the temperature in the strands (T_{St}) and in the conduit (T_{Jk}) are

$$\begin{aligned} A_{St} \rho_{St} C_{St} \frac{\partial T_{St}}{\partial t} - A_{St} \frac{\partial}{\partial x} \left(K_{St} \frac{\partial T_{St}}{\partial x} \right) = -Q_{He,St} \\ + Q_{Joule,St} + Q_{ext,St} - Q_{St,Jk} \end{aligned} \tag{9}$$

$$\begin{aligned} A_{Jk} \rho_{Jk} C_{Jk} \frac{\partial T_{Jk}}{\partial t} - A_{Jk} \frac{\partial}{\partial x} \left(K_{Jk} \frac{\partial T_{Jk}}{\partial x} \right) = -Q_{He,Jk} \\ + Q_{Joule,Jk} + Q_{ext,Jk} + Q_{St,Jk}, \end{aligned} \tag{10}$$

where A_{St} and A_{Jk} are the total cross sectional areas of the strands and conduit, ρ_{St} and ρ_{Jk} are the area averaged densities of the strand and conduit materials, C_{St} and C_{Jk} are the mass averaged specific heats, K_{St} and K_{Jk} are the area averaged conductivities. The linear heat sources densities represent the heat exchanged to the helium ($Q_{He,St}$ and $Q_{He,Jk}$ as defined in Eq. (8)), the Joule heat production in strands and conduit ($Q_{Joule,St}$ and $Q_{Joule,Jk}$) and the external heat sources ($Q_{ext,St}$ and $Q_{ext,Jk}$). A last term $Q_{St,Jk}$ takes into account the possibility for direct heat exchange between the strands and the conduit, at their contact surface $p_{St,Jk}$ and is defined as

$$Q_{St,Jk} = p_{St,Jk} h_{St,Jk} (T_{St} - T_{Jk}), \tag{11}$$

where the heat transfer coefficient $h_{St,Jk}$ has the physical meaning of a thermal resistance at the contact.

2.3. *Coupled System of Equations for the CICC*

The system described by the equations above is schematically represented in Fig. 2, where the structure and the degrees of freedom of the discretization adopted later on are also indicated. We can now write the system of equations to be solved in the matrix form

$$\mathbf{m} \frac{\partial \mathbf{u}}{\partial t} + \mathbf{a} \frac{\partial \mathbf{u}}{\partial x} - \frac{\partial}{\partial x} \left(\mathbf{g} \frac{\partial \mathbf{u}}{\partial x} \right) - \mathbf{s}\mathbf{u} = \mathbf{q}, \tag{12}$$

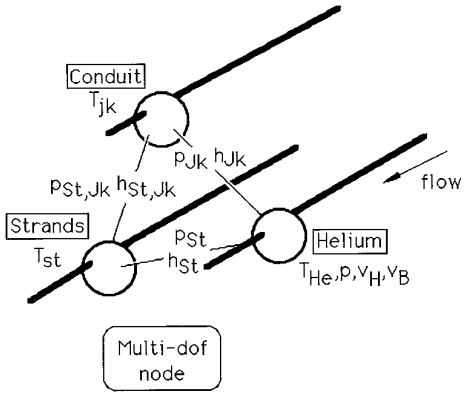

FIG. 2. Schematic representation of the components and their mutual thermal coupling (the links connecting them) in the model developed. The schematic picture shows the degrees of freedom identified and the discretization adopted within the cable cross section.

where the vector of unknown $\mathbf{u}$ is defined as

$$\mathbf{u} = \begin{bmatrix} v_B \\ v_H \\ p \\ T_{He} \\ T_{St} \\ T_{Jk} \end{bmatrix} \tag{13}$$

and the remaining matrices and vectors are defined as

$$\mathbf{m} = \begin{bmatrix} 1 & 0 & 0 & 0 & 0 & 0 \\ 0 & 1 & 0 & 0 & 0 & 0 \\ 0 & 0 & 1 & 0 & 0 & 0 \\ 0 & 0 & 0 & 1 & 0 & 0 \\ 0 & 0 & 0 & 0 & A_{St}\rho_{St}C_{St} & 0 \\ 0 & 0 & 0 & 0 & 0 & A_{Jk}\rho_{Jk}C_{Jk} \end{bmatrix} \tag{14}$$

$$\mathbf{a} = \begin{bmatrix} v_B & 0 & \frac{1}{\rho} & 0 & 0 & 0 \\ 0 & v_H & \frac{1}{\rho} & 0 & 0 & 0 \\ a_B\rho c^2 & a_H\rho c^2 & v & 0 & 0 & 0 \\ a_B\phi T_{He} & a_H\phi T_{He} & 0 & v & 0 & 0 \\ 0 & 0 & 0 & 0 & 0 & 0 \\ 0 & 0 & 0 & 0 & 0 & 0 \end{bmatrix} \tag{15}$$

$$\mathbf{g} = \begin{bmatrix} 0 & 0 & 0 & 0 & 0 & 0 \\ 0 & 0 & 0 & 0 & 0 & 0 \\ 0 & 0 & 0 & 0 & 0 & 0 \\ 0 & 0 & 0 & 0 & 0 & 0 \\ 0 & 0 & 0 & 0 & A_{St}K_{St} & 0 \\ 0 & 0 & 0 & 0 & 0 & A_{Jk}K_{Jk} \end{bmatrix} \tag{16}$$

$$\mathbf{s} = \begin{bmatrix} -\frac{2f_B|v_B|}{D_{hB}} & 0 & 0 & 0 & 0 & 0 \\ 0 & -\frac{2f_H|v_H|}{D_{hH}} & 0 & 0 & 0 & 0 \\ 2\rho\phi a_B f_B \frac{v_B|v_B}{D_{hB}} & 2\rho\phi a_H f_H \frac{v_H|v_H}{D_{hH}} & 0 & -\frac{\phi(p_{St}h_{St} + p_{Jk}h_{Jk})}{A_{He}} & \frac{\phi p_{St}h_{St}}{A_{He}} & \frac{\phi p_{Jk}h_{Jk}}{A_{He}} \\ 2\frac{a_B f_B}{C_v}\frac{v_B|v_B}{D_{hB}} & 2\frac{a_H f_H}{C_v}\frac{v_H|v_H|}{D_{hH}} & 0 & -\frac{\phi(p_{St}h_{St} + p_{Jk}h_{Jk})}{A_{He}\rho C_v} & \frac{p_{St}h_{St}}{A_{He}\rho C_v} & \frac{p_{Jk}h_{Jk}}{A_{He}\rho C_v} \\ 0 & 0 & 0 & p_{St}h_{St} & -p_{St}h_{St} - p_{St,Jk}h_{St,Jk} & p_{St,Jk}h_{St,Jk} \\ 0 & 0 & 0 & p_{Jk}h_{Jk} & p_{St,Jk}h_{St,Jk} & -p_{Jk}h_{Jk} - p_{St,Jk}h_{St,Jk} \end{bmatrix} \tag{17}$$

$$\mathbf{q} = \begin{bmatrix} 0 \\ 0 \\ 0 \\ 0 \\ Q_{\text{Joule,St}} + Q_{\text{ext,St}} \\ Q_{\text{Joule,Jk}} + Q_{\text{ext,Jk}} \end{bmatrix}. \quad (18)$$

The **a** matrix contains the only non-self-adjoint terms and can be shown to describe the wave propagation phenomena in the helium. The matrix **g** contains the diffusive contributions (only in strands and conduit), while the matrix **s** defines the source terms showing an explicit dependence (at least linear) on the system variables. Finally the vector **q** contains the external source terms, which can be implicitly and non-linearly dependent on the system variables (as for the Joule heating). Note that source terms defined by **s** are all expressed in the primary helium variables and are therefore directly amenable of implicit numerical treatment.

2.4. *Source Terms*

The heat generation in the strands and in the conduit is either due to external sources or to the Joule heating in the regions where the operating current is higher than the current carrying capacity of the superconductor. The external heat sources in the strands and in the conduit are due to movements and stress release, electromagnetic losses due to field changes, nuclear heat sources or external radiation, and conduction sources [10]. They are general in nature and provide the initial energy input causing the thermal transient. They are not specified further and are intended as the free parameter for the determination of the stability of the cable to external perturbation [2]. Note that for generality the heat generation terms in strands and conduit are kept separate, thus allowing for the possibility of investigating the different effects of heating the strands (as it is the case for AC losses in superconducting cables [10]) or the structure (as typically happens when heat sources external to the magnets or nuclear heating are applied [11]).

Neglecting the current redistribution transients it is possible to calculate the Joule heat deposited in the stabilizer, in the superconductor, and, in principle, in the conduit in the general case of arbitrary critical current density dependence on temperature and field [4]. The procedure is fully described in Ref. [4] and is therefore not given here.

2.5. *Transport Coefficients and Correlations*

The description of the model for the quenching CICC must be completed by giving explicit forms of the transport coefficients (i.e., the friction factors and heat transfer coefficient). The friction factors and the heat transfer coefficients of bundle and hole are specified through correlations, based on experimental measurements and appropriate fits. Typical correlations for helium flow in CICCs can be found in Refs. [12–15].

The description of the direct contact among strands and conduit, i.e., the coefficients $p_{\text{St,Jk}}$ and $h_{\text{St,Jk}}$, requires much empiricism. An equivalent heat transfer coefficient, playing the role of the thermal resistance at the contact, is assigned to model, at least to the first order, this effect. The contact perimeter depends on the void fraction and strand size in the bundle and can be of the order of 50% of the inner conduit perimeter [16]. While a direct measurement of the contact perimeter is possible (i.e., using optical scanning of a cross section), the contact resistance is unknown and, therefore, can only be taken as a parameter for sensitivity studies.

2.6. *Boundary and Initial Conditions*

The system needs a consistent set of boundary conditions to allow its solution. In a coil each cable length is connected to (large) inlet and outlet plena which provide constant pressure and temperature ambient conditions. The helium flow is usually in subsonic conditions, at Mach numbers of the order of 0.1 during a quench and well below in normal operation. According to a linearised characteristic analysis [17], for the helium flow it is therefore necessary to prescribe two Riemann variables at inflow and one at outflow sections. As the use of Riemann variables is not straightforward with the present selection of variables for the flow (p, v, T), the choice preferred here is to impose at inlet cross sections pressure and temperature (2 variables), and at outlet cross sections only pressure (1 variable). Note that during a quench, because of pressure waves propagation, inflow and outflow sections must be determined depending on the sign of the flow velocity. For the variables that cannot be specified at inflow/outflow sections a *free flow* condition is used, assuming that the variable does not change through the boundary. This condition is explicitly imposed only when balancing diffusion is present in the discretized equation, setting the boundary flux equal to zero. This procedure has been found to be stable and to provide a useful mean to impose physically known (i.e., measured) boundary conditions to the helium.

For the conduction equation in the cable, an assumption is made that the cable ends (strands and conduit) are adiabatic; i.e., the conduction heat flux at the boundary is zero. This is physically justified by the fact that in a *good* coil design the heat flux through the current leads, at the cable ends, must be kept as small as possible to decrease the steady state heat loss from room temperature. This condition, namely $\partial T/\partial x = 0$, is imposed *naturally* by the finite

elements technique used in the space discretization (see Section 3.2).

Finally, the initial conditions are those of unperturbed flow under a specified pressure drop (computed approximately from the incompressible limit of Eqs. (2) and (3), with linear pressure drop along the length of the cable) and equal temperature in the cable components (no steady state temperature gradient within a cross section).

3. NUMERICS AND SOLUTION ALGORITHM

3.1. *General Remarks*

The model discussed in the previous section is apparently physically simple, but it poses some remarkable problems in the selection of the numerical algorithm for its solution. The first difficulty is connected with the mathematical nature of the system of equations. The homogeneous part of the helium mass, momentum, and energy balances form a first-order hyperbolic system. In their conservative form they are equivalent to the system of 1D Euler equations for the flow of a compressible fluid [18]. This is the case when the flow velocity is small and the inertial terms are large, i.e., for early times in the transients. As the flow develops, the velocity increases and the viscous dissipation dominates in the momentum balance. This condition leads, after proper manipulation of the equation system, to a non-linear parabolic equation for the evolution of pressure. This indicates that the equation system loses its hyperbolic character as the dominance of the viscous term increases. It is important to note that this transition takes place continuously during the transience.

The equations describing the heat conduction in the strands and jacket are in any case of parabolic nature, although the large coupling term to the helium temperature tends to drive the temperature evolution of both. This strong thermal coupling of the strand and jacket temperature with the helium temperature results in a second numerical problem. The order of magnitude of the time constants for the evolution of the temperature difference between components is given by the ratio of the heat capacity to the heat transfer flux (using symbols in analogy with the previous definition):

$$\tau = \frac{pAC}{ph}$$

and has typical values of the order of a fraction of a millisecond for the strands in the cable (which has generally the smallest heat capacity and the highest convection heat flux at the wetted surface). This compares to the typical time constants of the quench evolution, around some seconds to some tens of seconds, and shows how the system obtained coupling strands and helium is of *stiff* mathematical nature.

A further problem is represented by the propagation of the normal zone. Due again to the strong thermal coupling, the temperature of the strand follows closely that of the helium at the normal front, so that a discontinuity in the temperature and density is present at the front, as shown in Ref. [7]. The transition to the normal conducting state causes a threshold rise of the Joule heating, and the moving front leads therefore to a problem of the free-boundary type. As shown in Refs. [7, 8], a fine discretization of this region is necessary to resolve the transition accurately and thus to properly compute the propagation speed of the front (typical mesh size below 1 cm).

Finally, the material properties (heat capacities, thermal conductivities, and electrical resistivities) in the temperature range of interest are highly non-linear. As an example, the heat capacity of metals changes in the range of 5 to 50 K approximately with the third power of the absolute temperature, while the copper resistivity rises with approximately the fifth power of temperature between 20 and 50 K [19]. The helium is in close vicinity to its critical point, and a pseudo-phase transition causes a large (one order of magnitude) change in density and specific heat [20]. Accurate interpolation of measured properties in the conditions of interest can be a heavy computational burden.

Although much effort has been devoted in past times to the solution of each of the above issues (parabolic/hyperbolic equations, stiffness, free boundary, non-linearity), no standard numerical method is known to treat optimally their *ensemble* in the form presented here. More specific to the previous work on quench simulation, as referenced in Section 1, a major difficulty often encountered was the computational burden associated both to explicit methods [4–6], because of the necessity to operate them at very small time steps for stability (in the microseconds range for a mesh size of 5 mm), and implicit procedures [3, 7], because of the complexity in the evaluation of the jacobians, their inversion, and iterations.

The novelty of the numerical implementation discussed here is in the application or adaption of known techniques to deal more efficiently with the problem. In particular, finite elements have been chosen for the discretization in space, finite differences for time marching. The choice has been guided by the generality and flexibility of these methods. A balancing diffusion is used on those equations which need stabilisation (convection dominated). A crude linearization was accepted in view of the small time steps forced by the necessity of tracking the free boundary motion. The variable selection for the helium flow, and in particular the use of temperature and pressure as thermodynamic variables, allowed implicit treatment of the stiff terms (temperature coupling and sound waves) and thus increased dramatically the stability of the time integration. This allowed us to retain in the model all fast modes at no penalty on the time stepping. Finally, space and time

adaptivity provided a boost to the code efficiency. The next sections describe the details of these choices.

3.2. *Space Discretization*

The space discretization scheme adopted here for the solution of Eq. (12) uses the finite elements method (FEM) [21]. Defining a nodal approximation $\mathbf{U}_i$ of the variables $\mathbf{u}$ using the following interpolation based on linear shape functions $\mathbf{N}_i$:

$$\mathbf{u} \approx \mathbf{N}_i \mathbf{U}_i$$

and writing the system of Eqs. (12) as a weighted residual at the nodes, with weight functions identical to the shape functions, we obtain the following semi-discrete system of ordinary differential equations in time

$$\mathbf{M}\frac{\partial \mathbf{U}}{\partial t} + (\mathbf{A} + \mathbf{G} - \mathbf{S})\mathbf{U} = \mathbf{Q}, \tag{19}$$

where the matrices $\mathbf{M}, \mathbf{A}, \mathbf{G}, \mathbf{S}$ and the vector $\mathbf{Q}$ are defined as the following integrals over the conductor length L:

$$\mathbf{M} = \int_L \mathbf{N}^T \mathbf{m} \mathbf{N}\, dx \tag{20}$$

$$\mathbf{A} = \int_L \mathbf{N}^T \mathbf{a} \frac{\partial \mathbf{N}}{\partial x}\, dx \tag{21}$$

$$\mathbf{G} \int_L \frac{\partial \mathbf{N}^T}{\partial x} \mathbf{g} \frac{\partial \mathbf{N}}{\partial x}\, dx \tag{22}$$

$$\mathbf{S} = \int_L \mathbf{N}^T \mathbf{s} \mathbf{N}\, dx \tag{23}$$

$$\mathbf{Q} = \int_L \mathbf{N}^T \mathbf{q}\, dx. \tag{24}$$

The matrices and vectors above are non-linear, as they depend on the material properties and on the solution.

The symmetric weighting used above is known to be optimal for self-adjoint problems (e.g., space discretization of a parabolic equation) but is *sub-optimal* for first-order hyperbolic problems, such as the system of Euler equations. This fact is indicated by the appearance of oscillations at sharp fronts. For such problems upwind methods (e.g., Petrov–Galerkin weighting, Taylor Galerkin, characteristic-Galerkin) are known to lead to better answers [18, 21–24]. Still, the mathematical complexity of the coupled system of Eqs. (12), which present both hyperbolic and parabolic aspects, does not allow a clear-cut selection.

The method chosen here is to correct the oscillatory behaviour using an additional, *balancing* diffusion. For scalar convection with velocity v, it has been shown [25, 26] that non-oscillatory solutions are obtained adding to the space-centered discretization an artificial diffusion g_u,

$$g_u = \frac{|v|\Delta x}{2}, \tag{25}$$

where Δx is the size of the space discretization (assumed uniform throughout the mesh). The scheme obtained in this case is the well known (first-order) upwind differencing [18]. Several justifications have been given to this additional diffusion, which balances the *negative* numerical diffusion introduced by central differencing of the first-order space derivative [27]. In the FEM context it can be interpreted as the effect of a non-symmetric weighting of the residuals [28], or it can be shown to be equivalent to the symmetrization of the original problem obtained using a variable change [29].

In order to determine the necessary amount of diffusion, and its vector form, we borrow from the *split* algorithms [30–32] the idea to separate the modes of the system of equations and to treat separately the fast modes (sound waves) and the slow modes (convection). In our case an eigenvalue analysis shows that the sound modes for system of Eqs. (12) are determined by the off-diagonal terms of matrix $\mathbf{a}$ (of Eq. (15)), while the convection modes are related only to the diagonal terms of $\mathbf{a}$. The sound propagation is associated to an equivalent second-order hyperbolic problem (i.e., self-adjoint) for which therefore we do not add numerical diffusion. The balancing diffusion is determined from the diagonal of $\mathbf{a}$, i.e., the convection velocities for each flow. The simple procedure adopted here is therefore to use the symmetric weighting and to add to the system (12) the diagonal diffusion

$$\mathbf{g}_u = \begin{bmatrix} \alpha_B \frac{|v_B|\Delta x}{2} & 0 & 0 & 0 & 0 & 0 \\ 0 & \alpha_H \frac{|v_H|\Delta x}{2} & 0 & 0 & 0 & 0 \\ 0 & 0 & \alpha_p \frac{|v|\Delta x}{2} & 0 & 0 & 0 \\ 0 & 0 & 0 & \alpha_T \frac{|v|\Delta x}{2} & 0 & 0 \\ 0 & 0 & 0 & 0 & 0 & 0 \\ 0 & 0 & 0 & 0 & 0 & 0 \end{bmatrix} \tag{26}$$

which clearly acts only on the helium equations and represents the direct extension of the artificial upwinding diffusion for the scalar model problem, given by Eq. (26). The

diffusion coefficient $\mathbf{g}$ in Eq. (12) is replaced by $(\mathbf{g} + \mathbf{g}_u)$ and accordingly the matrix $\mathbf{G}$ of Eq. (22) will contain the upwinding contribution. The parameters α_i must be chosen in the interval [0 ... 1] and control the artificial damping of the scheme. Any choice of α_i different from 0 will produce a first-order accurate algorithm, while only for a choice of $\alpha_i = 0$ it is possible to achieve global second-order accuracy (in a linear problem, at the penalty of an oscillatory solution). The freedom in the independent selection of α_i can be exploited to perform a *selective* upwind of the different equations. In particular, as the propagation of pressure waves is of secondary importance for the study of quench propagation (see the examples presented later), we can damp strongly the momentum balances and the pressure (continuity) equation selecting $\alpha_H = \alpha_B = \alpha_p = 1$ while the temperature (energy) equation can be integrated with $\alpha_T = 0$ to produce more accurate results.

It is interesting to compare the amount of numerical diffusion introduced in the scheme to the physical diffusion present in the problem, to show that, in reasonable conditions, the effect of the numerical stabilization does not affect the results of the simulation. As already said, typical mesh sizes needed to resolve the temperature gradients are in the order of 5×10^{-3} m [7, 8], and typical helium flow velocity is in the order of 1 m/s. Therefore the *numerical* diffusivity added to the problem would be in the order of 2.5×10^{-3} m^2/s. This compares, for a CICC as the one in Fig. 1, to a *physical* diffusivity (at the quench front) of the order of 1×10^{-2} m^2/s. Although the orders of magnitude are similar, this comparison shows that the mesh size needed to resolve the features in the solutions also guarantees that the effect of the numerical diffusion is tolerable.

3.3. *Time Discretization*

The non-linear ODE system Eq. (19) is integrated in time using a standard θ-implicit finite difference approximation,

$$\left.\frac{\partial \mathbf{U}}{\partial t}\right|^{n+\theta} = (1-\theta)\left.\frac{\partial \mathbf{U}}{\partial t}\right|^{n} + \theta\left.\frac{\partial \mathbf{U}}{\partial t}\right|^{n+1} \approx \frac{\mathbf{U}^{n+1} - \mathbf{U}^{n}}{\Delta t}, \quad (27)$$

where the time derivative of the variable $\mathbf{U}$ is approximated at time $n + \theta$ (with θ in the interval [0 ... 1]) using the values at times n and $n + 1$. The approximation above is known to be first-order accurate for any choice of θ, apart from the case $\theta = \frac{1}{2}$ when a second-order approximation is produced. More accurate methods could be used, based on more than two time stations. The advantage of the θ-implicit scheme chosen here is that the time step adaption discussed later does not require additional interpolations/extrapolations.

Using the approximation (27) in Eq. (19) we obtain finally the following system of non-linear algebraic equations,

$$\left[\frac{\mathbf{M}^{n+\theta}}{\Delta t} + \theta(\mathbf{A}^{n+\theta} + \mathbf{G}^{n+\theta} - \mathbf{S}^{n+\theta})\right] \Delta\mathbf{U} = \mathbf{Q}^{n+\theta} - (\mathbf{A}^{n+\theta} + \mathbf{G}^{n+\theta} - \mathbf{S}^{n+\theta})\mathbf{U}^{n} \quad (28)$$

for the time increments of the variable $\Delta\mathbf{U}$, defined as

$$\Delta\mathbf{U} = \mathbf{U}^{n+1} - \mathbf{U}^{n}.$$

3.4. *Linearisation and Stability*

The matrices and vectors in Eq. (28) depend on the solution, and in principle for any $\theta \neq 0$ an iterative technique would be necessary. We choose here to linearise the problem computing the matrices based on the solution obtained at time n, neglecting their variation in time, so that the algebraic system of equations to be solved is now:

$$\left[\frac{\mathbf{M}^{n}}{\Delta t} + \theta(\mathbf{A}^{n} + \mathbf{G}^{n} - \mathbf{S}^{n})\right] \Delta\mathbf{U} = \mathbf{Q}^{n} - (\mathbf{A}^{n} + \mathbf{G}^{n} - \mathbf{S}^{n})\mathbf{U}^{n}. \quad (29)$$

The system (29) is solved by direct inversion of the matrix at the l.h.s. Note that because of the neglect of the changes in the matrices in Eq. (29) we can formally obtain only first-order time-accuracy. We justify this choice *a posteriori* as, once more, the time step is forced to relatively small values by the necessity to follow the motion of the propagating front.

Unconditional linear stability is obtained, as usual, for any choice of $\theta \geq \frac{1}{2}$, including the influence of source terms which depend linearly on the solution (e.g., temperature coupling). In the non-linear case, test problems have shown that stable (but inaccurate) integration can be obtained using $\theta = 1$ at extremely high Courant numbers (of the order of 10^4 and above). We attribute this exceedingly large stability domain to the use of pressure as one of the thermodynamic variables. An analysis of the stability and convergence properties of this algorithm is in progress [38].

3.5. *Adaptive Meshing*

In order to resolve the temperature gradients at the propagating front, it is necessary to use typical mesh sizes in the fraction of centimeter range [7, 8]. This compares to flow path lengths of the order of 100 to 1000 m. A uniformly refined mesh could require therefore as many as 10^5 to 10^6 nodes to obtain an acceptable solution. Clearly this is not acceptable from the point of view of memory occupation and CPU time, also, because while in close vicinity of the propagating front the gradients in the solu-

tion are large, in the rest of the flow path the mesh required for accuracy reasons is much coarser. Adaptivity is the clear answer to this problem.

Most of the latest development in adaptive meshing has been devoted to steady state problems [33]. Once an error estimator has been defined, the mesh is adapted based on the error distribution in the equilibrium reached. For transients the mesh adaption can be more involved, as in principle each time step represents an *equilibrium* to be achieved within a specified error in the space discretization. The mesh adaption thus would involve a repetition of the step and, possibly, iterations.

In the case of quench simulation the selection of the error indicator is not straightforward. The problem is not self-adjoint, and an energy norm does not give any bound [22]. In addition, iterations are costly for a non-linear problem and should be avoided when necessary. On the other hand, experience shows that most of the numerical error can be introduced by a wrong propagation of the quench fronts [8], whose position and velocity appear to be the critical indicators for the quality of the solution. As we indeed have a clear definition of the moving boundary at each time step—the transition from superconducting to normal-conducting can be located in an element—we can avoid to use a general purpose error control procedure to localise the regions to be refined. We rather try to generate a fine mesh in close vicinity of the front and decrease the mesh density with increasing distance from the front.

In particular, at each time step an *ideal* mesh density distribution is generated over the existing mesh. The mesh density (d) distribution chosen here is given by a gaussian profile centered at the normal front location x_q, with maximum and minimum densities $d_{\max}$, $d_{\min}$ assigned by the user:

$$d = \max\left\{d_{\min}; d_{\max} e^{-(x-x_q)^2/2\sigma^2}\right\}. \tag{30}$$

The width of the gaussian profile σ governs the number of elements used in the refinement around each front and can be either prescribed or set automatically as a fraction β of the maximum allowed element size,

$$\sigma = \beta \frac{1}{d_{\max}},$$

so to guarantee that even in the worst case of a refinement required on an element of the maximum allowed size a smooth mesh is generated.

In the presence of several fronts the resulting density distributions are taken as the upper envelope of all gaussians. The element density is then used to generate the new mesh. The main issue at this stage is the interpolation of the variables from the old mesh to the new one. The approach chosen is to define a background *hard* mesh (the initial mesh) which cannot be modified and to refine or coarsen the mesh, according to the desired element density, inserting or removing *soft* nodes by successive element bisection or element joining. This guarantees that the interpolation in regions where the mesh is refined always satisfy the previous FE solution, while the coarsening never loses the initial features of the mesh. This procedure was found to give the best results for transient solutions. Note that as the minimum and maximum element sizes are given by the user, no direct control on the absolute magnitude of the error is possible. Work is in progress to define the a priori dependence of the error in the propagation velocity on the mesh (and time step) size.

Using this front-tracking procedure explicitly, i.e., at the end of each time step to predict the mesh to be used for the next step, no iteration is performed. The order of magnitude of the time step selected (see next section) allows generally an accurate prediction of the mesh.

3.6. *Adaptive Time Step Selection*

The key objective of this section is to have a simple time step control to achieve (approximately) the desired accuracy, avoiding iterations and repetitions of the step. To achieve this, we write the homogeneous part of the ODE system (19) in the form using the matrix of eigenvalues Λ and the characteristic variables $\mathbf{r}$ of the problem:

$$\frac{\partial \mathbf{r}}{\partial t} + \Lambda \mathbf{r} = 0, \tag{31}$$

where by definition ($\mathbf{X}$ is the matrix of the right eigenvectors) we have that

$$\Lambda = \mathbf{X}^{-1}[\mathbf{M}^{-1}[\mathbf{A} + \mathbf{G} - \mathbf{S}]]\mathbf{X}$$
$$\mathbf{r} = \mathbf{X}^{-1}\mathbf{U}.$$

Equation (31) is a system of decoupled ODEs in time, and the problem thus reduces to the time integration of a scalar equation for each degree of freedom of the problem:

$$\frac{\partial r_i}{\partial t} + \lambda_i r_i = 0. \tag{32}$$

Assuming constant λ_i during a time step, the θ-implicit finite difference discretization of Eq. (32) gives the numerical amplification factor,

$$A = \frac{r_i^{n+1}}{r_i^n} = \frac{1 - \lambda_i(1-\theta)\,\Delta t}{1 + \lambda_i \theta\,\Delta t} \tag{33}$$

which compares to the exact amplification factor

$$A^{ex} = e^{-\lambda_i \Delta t}. \tag{34}$$

The relative error (for a single step), defined as

$$\varepsilon(\lambda_i \Delta t) = \left| \frac{A}{A^{ex}} - 1 \right| = \left| \frac{1 - \lambda_i(1-\theta)\,\Delta t}{e^{-\lambda_i \Delta t}(1 + \lambda_i \theta\, \Delta t)} - 1 \right|,$$

can then be limited to a set maximum $\varepsilon_{\max}$ by appropriate selection of the product of $\lambda_i\ \Delta t$, solving the inequality

$$\left| \frac{1 - \lambda_i(1-\theta)\,\Delta t}{e^{-\lambda_i \Delta t}(1 + \lambda_i \theta\, \Delta t)} - 1 \right| \le \varepsilon_{\max}. \tag{35}$$

Equation (35) is non-linear, but it must be solved only once to determine the *optimal* value of the product $\lambda_i\, \Delta t_{\text{opt}}$ (i.e., the one giving at most an error $\varepsilon_{\max}$ per time step). The time step to be taken at a certain time t is then determined by corresponding value of λ_i,

$$\Delta t(t) = \frac{\lambda_i\, \Delta t_{\text{opt}}}{\lambda_i(t)}. \tag{36}$$

Equation (36) is used after the end of a step to estimate the following time step to be taken. The difficulty in the above procedure consists clearly in the evaluation of the decomposition of the system in the form of Eq. (32). As we are only searching for an approximate error control procedure, we assume here that the eigenvalues of equation i can be approximated at each time as

$$\lambda_i \approx -\frac{1}{u_i}\frac{\partial u_i}{\partial t} \approx -\frac{1}{U_i}\frac{\Delta U_i}{\Delta t}, \tag{37}$$

where u_i represents the ith variable in the system and U_i is its discrete counterpart (note that the approximation above is valid only for a diagonal system).

The accuracy criterion is equivalent to a limit on the maximum relative variation of the variable u_i during one time step and shows relation to the work reported in Ref. [34]. A final important remark is that, as we are not primarily interested in the pressure wave propagation for quench simulations, we can restrict the accuracy control to the temperature evolutions. Therefore at each time step the estimated eigenvalues for the helium, strand, and conduit temperatures are evaluated using Eq. (37). The time step width is adapted according to the result of the accuracy control. As for the mesh adaption, the simple prediction of the new time step has been found to work satisfactorily (no iteration is performed).

4. VERIFICATION OF THE MODEL

The model developed here is highly non-linear and its implementation rather complex. Therefore it is not easy to verify its validity, both from the point of view of the physical assumptions made and of the numerical implementation. Checks have been made against other existing computer codes and available experimental results. Unfortunately, up to now, no experimental results are available for the conductor geometry with central cooling hole to be used in ITER. For this reason all comparisons were restricted to single 1D flows. Data are available on supercritical helium cooling and quench propagation. Two comparisons have been selected and presented here. The first regards data on thermal induced flow produced in the HELITEX test facility at KfK [35], while the second is based on quench propagation in a small size CICC [36, 37].

4.1. *Comparion to the HELITEX Data from Ref.* [35]

The first test of the model presented here was performed on the rather old experimental data produced and analysed by Benkowitsch and Krafft [35] on transient induced flow in supercritical helium contained in a copper pipe. A 32-m long channel, with square cross section, was initially filled with stagnant supercritical helium. The inlet valve was closed and the experiment began as the stored energy of a capacitor bank was discharged in a resistive heater of 15 m length, located at the inlet. Pressure was recorded at various locations along the length. The main data for the geometry, friction factor, and heating pulses are reported in Table I. In the experiments, the input energy was taken as a parameter.

The maximum pressure measured at the sensors and the corresponding value computed are shown in Fig. 3. The calculations were performed using a fixed (i.e., not adaptive) 200 elements mesh and did not show mesh dependence below (100 elements) and above (400 elements) this size. As shown in Fig. 3, the maximum pressure increase is reproduced accurately within 15% over the whole input energy range. The deviation of measurements and simulation results increases at high input energies. In these conditions the temperature increase of the components surrounding the test section (valves, insulation) contributes significantly to the energy balance and thus decreases the maximum pressure as observed. Finally, a phase change was taking place during the experiment at the test section outlet, especially at higher input energies. This was only roughly taken into account using the gas density in the simulation as soon as the phase boundary was reached. Still, the agreement of simulation and measurement is satisfactory.

TABLE I

Data for the HELITEX Experiment by Benkowitsch and Krafft [35]

Copper tube geometry	
Channel length (m)	32
Helium cross section (mm^2)	4
Hydraulic diameter (mm)	2
Initial temperature (K)	4.14
Initial pressure (bar)	1.013

Friction factor

—Laminar regime,

$$f = \frac{7}{8}\frac{16}{\mathrm{Re}}$$

—Turbulent regime,

$$f = \frac{7}{8}\frac{0.076}{\mathrm{Re}^{0.25}}$$

Heat flux into the helium

$$Q_t(t) = \begin{cases} Q_0 \dfrac{t}{\tau_1} & \text{for } t \le \tau_1 \\ Q_0 e^{-(t-\tau_1)/\tau_2} & \text{for } t > \tau_1 \end{cases}$$

$$Q(x,t) = \begin{cases} Q_t(t) & \text{for } x \le 15 \\ 0 & \text{for } x > 15, \end{cases}$$

where the time constants are defined as

τ_1(ms)	77
τ_2(ms)	286

and the energy input and associated linear heat flux are

$E(J)$	$Q_0(W/m)$
25	4.816
50	9.632
75	14.464
100	19.260
150	28.892
200	38.520

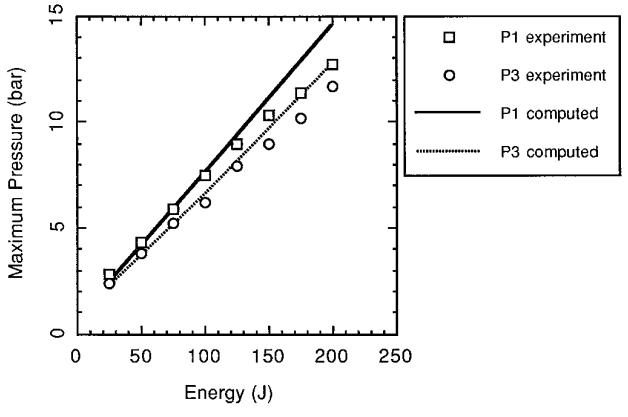

FIG. 3. Maximum pressure at the sensors P1 and P3 (at inlet and in the middle of the pipe) in the experiment of Ref. [35] as a function of the input energy as measured and computed.

TABLE II

Data for the Quench Propagation Experiment by Ando *et al.* [36, 37]

Conductor geometry	
Strand diameter (mm)	0.98
Number of strands	18
NbTi cross section (mm^2)	3.4
Copper cross section (mm^2)	10.2
Conduit (SS) cross section (mm^2)	25.1
Helium cross section (mm^2)	13.3
Wetted perimeter strands (mm)	55
Wetted perimeter conduit (mm)	19
Hydraulic diameter (mm)	0.69
Copper RRR (−)	60
Operating and critical conditions	
Magnetic field (T)	7
Temperature (K)	4.2
Pressure (MPa)	1.0
Massflow (g/s)	0.0
Critical temperature (K)	6.24
Critical current (kA)	3.0
Operating currents (kA)	1.5–2.0

Friction factor

—Laminar regime,

$$f = \frac{16}{\mathrm{Re}}$$

—Turbulent regime,

$$f_T = N \cdot 0.046\,\mathrm{Re}^{-0.25}$$

$$N = 3$$

4.2. *Comparion to the Quench Propagation Data from Refs.* [36, 37]

The experimental data measured by Ando *et al.* [36, 37] on quench propagation and pressure increase in a small size CICC were used as a second verification of the capabilities of the model. A conductor with the data reported in Table II was wound for a length of 26 m and inserted in a 7-T background field. Starting from the operating conditions given in Table II, a quench was initiated at different operating currents between 1.5 kA and 2 kA by firing a 4-cm long heater with a very fast pulse (0.1-ms nominal duration). The normal length evolution was monitored by means of voltage taps placed along the conductor length. A pressure sensor measured the pressure evolution in the centre of the normal zone.

For the simulation it was assumed that the conductor length was symmetric (i.e., only 13 m were analysed), with the open end at constant pressure, set at 1 MPa. An adaptive mesh with minimum mesh size of 1 mm and a total number of element in the order of 500 was used. The time step was adaptively chosen between 0.1 and 2.5 ms, but for most of the time the integrator operated at the maximum time step. Note that this corresponds to a Courant

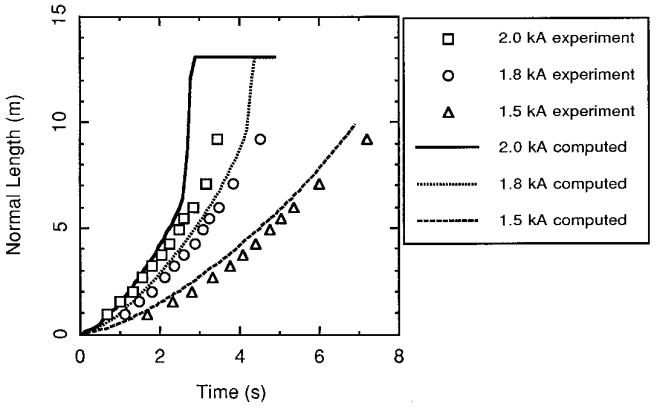

FIG. 4. Normal front location in the experiment of Ando *et al.* [36, 37] as measured (symbols) and computed (lines).

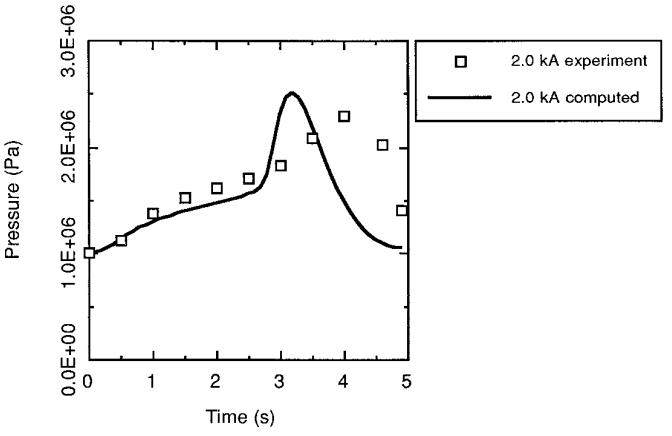

FIG. 5. Pressure in the centre of the normal zone in the experiment of Ando *et al.* [36, 37] as measured (symbols) and computed (lines).

number (based on the sound speed modes) between 500 and 1000 (depending on the temperature). A similar model, but based on an explicit time integrator [4], would therefore produce comparable results but with 1 to 2 orders of magnitude penalty on the CPU time, owing to the larger number of smaller time steps.

The friction factor was obtained correcting a smooth tube correlation by a factor of 3 (see Table II). The quench was initiated in the simulation by a heat input over 4 cm in the centre of the conductor length. The heating duration was 0.1 ms and the power was adjusted in order to just initiate the quench. In the first calculations it was observed that the quench propagated faster than measured, and that the propagation velocity had a strong dependence on the local value of the heat transfer coefficient at the normal front, especially during the initial phase. In fact, in the beginning of the quench, the helium has a low speed (below 1 m/s), and the propagation is due both to the helium front motion and to the heat flux through the strands along the conductor. The flow conditions for a normal zone with a length of some centimeters can be far from the range of validity of the 1D correlations. For this reason it was assumed here that the heat transfer coefficient between strands and helium could be significantly higher than computed by the 1D correlations, and a lower inferior limit for h was set at 2500 W/m^2K, in order to match the initial propagation data (in the interval 0 to 1 s) for the 2 kA case.

The results of the simulations compared to the experimental measurements are reported in Figs. 4 through 6. Figure 4 shows the location of the normal front in three cases (2 kA, 1.8 kA, and 1.5 kA). Considering the uncertainties in the description of the experiment, the agreement between measurement and simulation is excellent. In the 2-kA case the normal front accelerates after 2.2 s. A similar acceleration is seen in the measurement only at a later time (around 2.5 s) and can be attributed to a change in the propagation mode happening when the helium compression and frictional heating at the front increases the helium temperature up to the current sharing level, a phenomenon often called thermal-hydraulic quench back (THQB) [5]. This change in the propagation is confirmed by looking at the pressure traces (in Fig. 5) for the 2-kA case, where the pressure in the centre peaks because an increasing amount of helium is engulfed in the normal region. Note that the mismatch between the onset of THQB seen in the normal front location curves is the cause for the mismatch in the location of the peaks in the pressure traces. The onset of THQB was found to be critically dependent on the friction factor coefficient assumption (see Table II), where assuming, e.g., a correction factor $N = 2$ on the smooth tube correlation, no THQB was computed. This could be an indication that the value of the friction factor used in the simulation is slightly too high, a fact

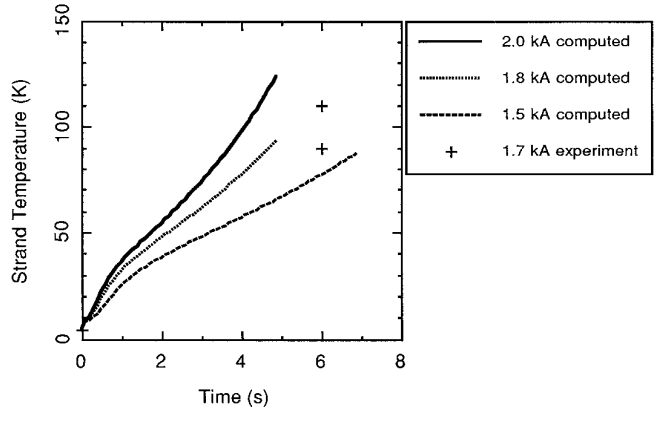

FIG. 6. Temperature of the cable in the centre of the normal zone in the experiment of Ando *et al.* [36, 37], as computed (lines) as a function of the operating current. The crosses are estimated values obtained from voltage reading for an operating current of 1.7 kA; A $\pm$ 10 K scattering is due to the uncertainty in the reading.

consistently confirmed by the presence of a THQB in the late times of the simulation for 1.8 kA which is not observed experimentally.

The computed pressure trace for the 2-kA case (in Fig. 5) appears initially too low compared to the measurement (apart from the THQB peak). A possible explanation could be that the boundary condition assumed for the calculation was of constant pressure at the exit, where in reality the pressure relief lines on the sample could introduce additional pressure gradients adding to the pressure value in the ambient where helium is discharged.

Finally, in Fig. 6 are shown the traces of the cable temperature in the centre of the sample. For this quantity no direct measurement is available. However, the measurement of voltage along the conductor adjacent to the heater can be used to deduce the copper resistivity and, from known scaling laws, the copper temperature. The estimated temperature for a 1.7-kA run is reported at 6 s as the two crosses in Fig. 6 (two adjacent taps were used for this estimate, giving a 20-K difference in the temperature computed). The values computed for 1.8 and 1.5 kA are correct above and below the estimated temperatures and indicate that the prediction is indeed in the correct range.

In summary it seems that, although the ideal representation based on the model discussed here is not fully satisfactory (e.g., the consideration on the boundary conditions, a slight variation of the operating current not taken into account in the simulation, the neglect of additional heat capacities external to the cable), this comparison shows that the inner consistency achieved by the simulations is good. Also, it is important to recognize that the propagation of the quench depends critically upon parameters that are not known with certainty (friction factor, heat transfer coefficient), and therefore any predictive application of this model can only be performed in conjunction with a parametric study on the influence of these critical parameters.

5. CONCLUSIONS

A model for the simulation of quench initiation and its evolution in the cable-in-conduit conductors being designed for ITER has been presented. The model includes a separate treatment of the hydraulics in the cable bundle and in the central cooling channel and properly describes the temperature differences within the components of the cable cross section. The numerical implementation has been discussed, showing that a low order implicit finite elements algorithm coupled with automatic time step and mesh size control gives satisfactory results in terms of accuracy and computational speed.

The main feature of the numerical method is that it is able to obtain stable results at extremely high Courant numbers (of the order and greater than 10^3) and therefore large time steps. This in turn allows small element sizes without penalty on the number of time steps. The stability of the algorithm in the solution of the fluid flow is mostly attributed to the direct use of pressure as a thermodynamic variable. To achieve this, the conservation equations have been written in a non-standard, non-conservative form without introducing approximations to the gas behaviour. The capability of time stepping on a time scale larger than the characteristic time of sound wave propagation gives, for typical simulations, a gain of 1 to 2 orders of magnitude CPU time compared to existing explicit solvers (as, e.g., the one of Ref. [4]). This model, however, in contrast to the results of Ref. [7] where sound waves and temperature gradients in a cross section are suppressed, retains generality and can be applied to conditions where these effects are important simply by time stepping on the appropriate time scale.

The solver presented here is currently used for the design and analysis of the ITER conductors [39]. Some examples of application have been reported to demonstrate the reliability of the code produced. Experimental results could be reproduced with satisfactory accuracy, although more work on the validation on the specific details of the treatment of the two flows is needed.

APPENDIX A: NON-CONSERVATIVE FORM OF THE HELIUM FLOW EQUATIONS

The flow of helium in long conductors is described by the 1D balances of mass, momentum, and energy for a compressible fluid with ignorable viscosity but significant friction at the wetted perimeter. In computational fluid-dynamics it is customary to use the conservative form of the flow equations, as only this form guarantees that the numerical fluxes respect the physical conservation laws [18]. Here we prefer to use a non-conservative form of the equation to allow direct coupling of the temperatures of the various components (the convective heat fluxes contain the temperatures explicitly). This choice is also guided by the fact that all superconductors examined will have a constant flow cross section along the length, so that no shock should appear in the solution. Temperature and pressure are taken as state variables. The first, temperature, is chosen—as already said—for homogeneity with the state variable of the strand and conduit and thus allow direct, implicit coupling of the energy balances. The second, pressure, is chosen because it improves greatly the non-linear stability properties of the numerical integration of the flow equations.

For a 1D channel with cross section A, hydraulic diameter D_h, friction factor f, and a linear heat flux Q, the conser-

vative form of the flow equations (for density ρ, mass flux ρv, and total energy density ρe) is

$$\begin{aligned}\frac{\partial \rho}{\partial t}+\frac{\partial(\rho v)}{\partial x}&=0\\ \frac{\partial(\rho v)}{\partial t}+\frac{\partial(\rho v^2)}{\partial x}+\frac{\partial p}{\partial x}&=-\rho F\\ \frac{\partial(\rho e)}{\partial t}+\frac{\partial[(\rho e+p)v]}{\partial x}&=\frac{Q}{A},\end{aligned}\tag{A1}$$

where the total specific energy e is the sum of specific internal energy i and specific kinetic energy $v^2/2$:

$$e=i+\frac{v^2}{2}$$

and the friction force at the wetted surface F is defined as

$$F=2f\frac{v|v|}{D_h}.$$

The system (A1) is identical to the 1D Euler equations [18] apart from the addition of the wall friction (in the momentum balance) and of the heat influx (in the energy balance).

The above system can be written in terms of pressure p, velocity v, and temperature T using the following thermodynamics relations

$$d\rho=\frac{1+\phi}{c^2}\,dp-\frac{\phi\rho}{c^2}\,dh\tag{A2}$$

$$di=\left(\frac{p}{\rho}-\phi C_v T\right)\frac{d\rho}{\rho}+C_v\,dT,\tag{A3}$$

where the coefficients C_v and c are respectively the specific heat at constant volume and the isentropic speed of sound in the helium, while ϕ is the Gruneisen parameter defined as

$$\phi=\left(\frac{\rho}{T}\frac{\partial T}{\partial \rho}\right)_S,$$

where the derivative is taken at constant entropy S. The Gruneisen parameter ϕ is equal to $\gamma-1$ for an ideal gas (γ is the ratio of specific heats). In Eq. (A2) the fluid specific enthalpy has been used, defined as

$$h=i+\frac{p}{\rho}.$$

Using the relations (A2)–(A3) and substituting into the conservative set (A1), we obtain the system of non-conservative equations for p, v, and

$$\begin{aligned}\frac{\partial v}{\partial t}+v\frac{\partial v}{\partial x}+\frac{1}{\rho}\frac{\partial p}{\partial x}&=-F\\ \frac{\partial p}{\partial t}+\rho c^2\frac{\partial v}{\partial x}+v\frac{\partial p}{\partial x}&=\phi\left(\frac{Q}{A}+\rho v F\right)\\ \frac{\partial T}{\partial t}+\phi T\frac{\partial v}{\partial x}+v\frac{\partial T}{\partial x}&=\frac{\dfrac{Q}{A}+\rho v F}{\rho C_v},\end{aligned}\tag{A4}$$

where the equation for pressure has taken the role of the mass continuity equation, while the energy equation is substituted by an equation for temperature. In this form the wall friction dissipation and the heat influx contribute to both mass and energy balances. In addition to the advantages quoted earlier, this form of the equations allows a direct specification of the boundary conditions on pressure and temperature, two variables that are directly measured in experiments.

The ITER CICCs have the particularity of a central cooling hole that allows large massflows at reduced pressure drop compared to CICCs without the additional cooling hole. The flow in such a geometry is more difficult to describe than in case of an homogeneous flow, as mass transfer takes place between the different regions of the cable. We assume here that the two flows can be treated as separate 1D channels with additional terms describing the mass, momentum, and energy transfer between them. In principle, even under the 1D simplifying assumptions, a system of six equations (continuity, momentum, and energy balances for each flow) coupled through mass, momentum, and energy exchange term should be solved for the helium flow. A first tentative reduction of this system was performed in Ref. [9], along the lines reported in the following.

The central cooling hole is separated from the bundle either by a perforated tube or a spiral which sustains the cable bundle. As one of the objectives is to maintain the good hydraulic contact of the two channels, the perforation is large compared to the helium cross section. This implies that the pressure loss in the transverse direction to the cable axis (i.e., from the bundle to the cooling hole) is small, and therefore pressure equilibration is fast (the typical time scale is that of the sound wave propagation transverse to the conductor, with characteristic length around 1 cm and time constants in the range of tens of microseconds).

The mass exchange and, therefore, the density equilibration, between the two flows takes place with characteristic times governed by the transverse flow velocity. Assuming that typical values of transverse velocity are in the same order of magnitude of the longitudinal velocity, typically

between 0.1 and 1 m/s, the time scale over a characteristic length of 1 cm is of the order of 10 to 100 ms.

The quench phenomenon evolves on a time scale of the order of seconds, and therefore it can be assumed that for quench propagation studies pressure and density in the two flow channels is the same. This implies that the thermodynamic state is the same and, therefore, all other thermodynamic variables will be equal, and in particular, temperature. Under this assumption it is possible to add the continuity and energy balances for the two flows. Assuming in addition that the momentum transfer among the two flows is small and that the contribution of the kinetic energy to the energy balance is also small (this is always verified for helium in subsonic, cryogenic conditions), we can reduce the original six equations to four balances: a global continuity equation (obtained by adding the single continuity equations of the flows) a global energy balance (obtained by adding the single energy balances), and the two independent momentum balances:

$$\begin{aligned}
&\frac{\partial \rho}{\partial t} + \frac{\partial (\rho v)}{\partial x} = 0 \\
&\frac{\partial (\rho v_{\mathrm{B}})}{\partial t} + \frac{\partial (\rho v_{\mathrm{B}}^2)}{\partial x} + \frac{\partial p}{\partial x} = -\rho F_{\mathrm{B}} \\
&\frac{\partial (\rho v_{\mathrm{H}})}{\partial t} + \frac{\partial (\rho v_{\mathrm{H}}^2)}{\partial x} + \frac{\partial p}{\partial x} = -\rho F_{H} \\
&\frac{\partial (\rho e)}{\partial t} + \frac{\partial [(\rho e + p) v]}{\partial x} = \frac{Q}{A}.
\end{aligned} \tag{A5}$$

In the equations above it must be noted how the density and energy are convected at the effective velocity of the homogenised flow, v, defined as in Eq. (5) in the main text. Now using the thermodynamic relations equations (A2) and (A3), we obtain the final set of non-conservative equations for the helium in terms of helium temperature, pressure, and flow velocities:

$$\begin{aligned}
&\frac{\partial v_{\mathrm{B}}}{\partial t} + v_{\mathrm{B}} \frac{\partial v_{\mathrm{B}}}{\partial x} + \frac{1}{\rho} \frac{\partial p}{\partial x} = -F_{\mathrm{B}} \\
&\frac{\partial v_{\mathrm{H}}}{\partial t} + v_{\mathrm{H}} \frac{\partial v_{\mathrm{H}}}{\partial x} + \frac{1}{\rho} \frac{\partial p}{\partial x} = -F_{\mathrm{H}} \\
&\frac{\partial p}{\partial t} + a_{\mathrm{B}} \rho c^2 \frac{\partial v_{\mathrm{B}}}{\partial x} + a_{\mathrm{H}} \rho c^2 \frac{\partial v_{\mathrm{H}}}{\partial x} + v \frac{\partial p}{\partial x} \\
&\qquad = \phi (a_{\mathrm{B}} v_{\mathrm{B}} F_{\mathrm{B}} + a_{\mathrm{H}} v_{\mathrm{H}} F_{\mathrm{H}}) + \frac{\phi Q}{A} \\
&\frac{\partial T_{\mathrm{He}}}{\partial t} + a_{\mathrm{B}} \phi T_{\mathrm{He}} \frac{\partial v_{\mathrm{B}}}{\partial x} + a_{\mathrm{H}} \phi T_{\mathrm{He}} \frac{\partial v_{\mathrm{H}}}{\partial x} + v \frac{\partial T_{\mathrm{He}}}{\partial x} \\
&\qquad = \frac{(a_{\mathrm{B}} v_{\mathrm{B}} F_{\mathrm{B}} + a_{\mathrm{H}} v_{\mathrm{H}} F_{\mathrm{H}})}{\rho C_v} + \frac{Q}{A \rho C_v}.
\end{aligned} \tag{A6}$$

The set above is the one used in the solution of the transient (note that in the text the total helium cross section is indicated by A_{He} and the linear heat flux is Q_{He}).

APPENDIX B: SYMBOLS AND NOTATION

The following symbols have been used in the text. Duplicate symbols have been reported for each entry used. Superscripts and subscripts are not indicated when they have obvious meaning in the text:

relative cross section of helium in the bundle and in the hole	a_{B}, a_{H}
matrix of convection coefficients	$\mathbf{a}$
cross section	A
amplification factor	A
discretized matrix of convection coefficients	$\mathbf{A}$
helium isentropic speed of sound	c
Courant number	C
specific heat	C
helium specific heat at constant pressure	C_{p}
helium specific heat at constant volume	C_{v}
mesh density	d
hydraulic diameter	D_{h}
helium total specific energy	e
helium friction factor	f
specific wall friction force	F
matrix of diffusion coefficients	$\mathbf{g}$
matrix of upwind diffusion coefficients	$\mathbf{g}_{\mathrm{u}}$
discretized matrix of diffusion coefficients	$\mathbf{G}$
heat transfer coefficient	h
helium specific enthalpy	h
helium internal specific energy	i
thermal conductivity	K
matrix of mass (time derivative) coefficients	$\mathbf{m}$
discretized matrix of mass (time derivative) coefficients	$\mathbf{M}$
nodal shape function	$\mathbf{N}$
helium pressure	p
wetted perimeter	p
source vector	$\mathbf{q}$
linear heat flux	Q
discretized source vector	$\mathbf{Q}$
characteristic variable	r
matrix of characteristic variables	$\mathbf{r}$
source matrix	$\mathbf{s}$
discretized source matrix	$\mathbf{S}$
time	t
temperature	T
unknown	u
vector of unknowns	$\mathbf{u}$
nodal unknown	U

vector of nodal unknowns	$\mathbf{U}$
velocity	v
length	x
matrix of right eigenvectors	$\mathbf{X}$
upwind parameter	α
mesh refinement extension parameter	β
mesh size (space step)	Δx
time step	Δt
vector of increments of the nodal unknowns	$\Delta\mathbf{U}$
relative error	ε
helium Gruneisen parameter	ϕ
ratio of specific heats in the helium	γ
eigenvalue	λ
matrix of eigenvalues	Λ
implicitness parameter for time integration	θ
density	ρ
gaussian width of mesh density distribution function	σ
time constant	τ

REFERENCES

1. R. J. Thome, *IEEE Trans. Mag.* **30**(4), 1595 (1994).
2. L. Bottura, *Fus. Eng. Des.* **20,** 351 (1993).
3. V. Arp, "Computer Analysis of Quench Transients in Force-Flow Cooled Superconductors for Large MHD Magnets," in *Proceedings, Superconducting MHD Magnet Design Conf., MIT, Cambridge, 1978.*
4. L. Bottura and O. C. Zienkiewicz, *Cryogenics* **32**(7), 659 (1992).
5. C. Luongo, R. J. Loyd, F. K. Chen, and S. D. Peck, *IEEE Trans. Mag.* **25**(2), 1589 (1989).
6. R. Wong, "Program CICC Flow and Heat Transfer in Cable-in-Conduit Conductors," in *Proceedings, 13th Symp. on Fus. Eng., Knoxville, 1989.*
7. A. Shajii and J. P. Freidberg, *J. Appl. Phys.* **76**(5), 3149 (1994).
8. L. Bottura and A. Shajii, *IEEE Trans. Appl. Sup.,* **5**(2), 495 (1995).
9. L. Bottura, *IEEE Trans. Appl. Sup.,* **5**(2), 745 (1995).
10. M. N. Wilson, *Superconducting Magnets,* (Clarendon Press, Oxford, 1983).
11. N. Mitchell, *IEEE Trans. Mag.* **30**(4), 1602 (1994).
12. H. Katheder, *Cryogenics* **34,** 595 (1994).
13. P. J. Giarratano, V. D. Arp, and R. V. Smith, *Cryogenics* **11,** 385 (1971).
14. W. B. Bloem, *Cryogenics* **26,** 300 (1986).
15. G. Krafft, "Heat Transfer Below 10 K," in *Cryogenic Engineering,* edited by B. A. Hands (Academic Press, New York, 1986), p. 171.
16. X. Cheng and W. Lehmann, KfK Report FZKA 5517, Karlsruhe, 1995 (unpublished).
17. W. J. Usab and E. M. Murman, "Embedded Mesh Solutions of the Euler Equations Using a Multiple-Grid Method," in *Adv. Comput. Transonics* (Pineridge Press, Swansea, 1985), p. 447.
18. C. Hirsch, *Numerical Computation of Internal and External Flows,* Vol. 1, (Wiley, New York, 1988).
19. R. P. Reed and A. F. Clark (Eds.), *Materials at Low Temperature* (ASM International, Materials Park, OH, 1983).
20. V. D. Arp and R. D. McCarty, NIST Technical Note 1334, 1989 (unpublished).
21. O. C. Zienkiewicz, *The Finite Element Method,* Vol. 2, 4th ed. (McGraw–Hill, New York, 1991).
22. R. Loehner, Ph.D. thesis, University of Wales, Dept. of Civil Eng., 1984 (unpublished).
23. J. Donea, *Int. Jour. Numer. Methods Eng.* **20,** 101 (1984).
24. O. C. Zienkiewicz, R. Loehner, K. Morgan, and J. Peraire, *Finite Element Fluids* **6,** 41 (1985).
25. B. P. Leonard, "A Survey of Finite Differences of Opinion on Numerical Muddling of the Incomprehensible Defective Confusion Equation," in *Finite Elements for Convection Dominated Flows,* edited by T. R. Hughes ed., AMD, Vol. 34, (ASME, New York, 1979).
26. I. Christie, D. F. Griffits, A. R. Mitchell, and O. C. Zienkiewicz, *Int. J. Numer. Methods Eng.* **10,** 1389 (1976).
27. J. Donea, *Nucl. Eng. Des.* **80,** 141 (1984).
28. N. Brooks and T. R. J. Hughes, *Comput. Methods Appl. Mech. Eng.* **32,** 199 (1982).
29. G. L. Guymon, V. H. Scott, and L. R. Herrmann, *Water Resources Res.* **6,** 1611 (1970).
30. A. J. Chorin, *Math. Comput.* **22,** 745 (1969).
31. J. Donea, S. Giuliani, H. Laval, and L. Quartapelle, *Comput. Methods Appl. Mech. Eng.* **30,** 53 (1982).
32. O. C. Zienkiewicz, J. Szmelter, and J. Peraire, *Comput. Methods Appl. Mech. Eng.* **78,** 105 (1990).
33. J. Peraire, M. Vahdati, K. Morgan, and O. C. Zienkiewicz, *J. Comput. Phys.* **72,** 449 (1987).
34. D. Givali and I. Henigsberg, *Comm. Numer. Methods Eng.* **9,** 873 (1993).
35. J. Benkowitsch and G. Krafft, *Cryogenics* **20,** 209 (1980).
36. T. Ando, M. Nishi, T. Kato, J. Yoshida, N. Itoh, and S. Shimamoto, *Adv. Cryo. Eng.* **35,** 701 (1990).
37. T. Ando *et al.,* "Experimental Investigation of Pressure Rise of Quenching Cable-in-Conduit Superconductor," in *Proceedings, 12th Int. Cryo. Eng. Conf., Southampton, 1988.*
38. R. Zanino, S. De Palo, and L. Bottura, *J. Fus. Energy,* **14**(1), 25 (1996).
39. M. Shimada and N. Mitchell, *J. Fus. Energy*, **14**(1) 59 (1996).